Communications

Precipitation and Aging in Al-Si-Ge-Cu

D. MITLIN, V. RADMILOVIC, U. DAHMEN, and J.W. MORRIS, Jr.

In commercial, Al-Cu based alloys, the elements Si, Mn, Be, Ge, Sn, Ag, and Cd have all been used to modify the dominant precipitation reaction.[1–11] One mechanism by which the precipitation reaction is altered is the preferential precipitation of alloy modifiers, producing heterogeneous sites that nucleate Al-Cu or Al-Cu-Mg precipitates.[3–5] It has been found[5,6] that trace additions of Sn, Cd, or In promote a dense and homogeneous distribution of fine θ' precipitates (a metastable form of the equilibrium θ phase, Al_2Cu). In the case of Sn, transmission electron microscopy (TEM) studies showed that the Sn precipitates first, providing heterogeneous sites for nucleation of θ'. We have recently shown that Si behaves in a similar way.[11] Inclusions such as Al_2O_3[12] or SiC particles[13] also change the precipitation kinetics, since they, or the misfit dislocations they introduce into the matrix, also serve as heterogeneous nucleation sites.

Recent studies of Al-Si-Ge alloys[14–19] have shown that the precipitates formed in Al-Si-Ge can be almost an order of magnitude smaller than those commonly found in binary Al-Si or Al-Ge. This is attributed to the fact that Si and Ge atoms have compensating volumetric strains in Al solid solution; Ge is larger than Al, while Si is smaller. The strain compensation promotes a dense distribution of Si-Ge solute clusters that transform to diamond cubic Si-Ge precipitates upon elevated temperature aging. The precipitates found in the ternary alloy are not only finer, but also more equiaxed than those in binary Al-Si or Al-Ge alloys.

Unfortunately, the Si-Ge precipitates do not form a sufficiently dense distribution to accomplish dramatic hardening.[15] The reason appears to be the high interfacial tension of the Si-Ge precipitates, which has the consequence that the solubility of Si and Ge in equilibrium with the precipitates remains relatively high, and the volume fraction of precipitates correspondingly low, until they have coarsened.[20]

While Si-Ge precipitates may not harden effectively in their own right, their dense distribution, compared to that of Si, Ge, or Sn, and their large lattice mismatch, once they have transformed into the diamond structure,[11] suggest that they would offer an excellent template of heterogeneous sites for the nucleation of θ' in a quaternary Al-Si-Ge-Cu alloy. The present work was done to explore that possibility. The results show that Al-Si-Ge-Cu alloys combine rapid precipitation hardening with high peak hardness and exceptional thermal stability.

D. MITLIN, Graduate Student and Research Assistant, and J.W. MORRIS, Jr., Professor of Metallurgy, are with the Department of Materials Science and Engineering, University of California, Berkeley, CA 94720, and the Center for Advanced Materials, Lawrence Berkeley National Laboratory, Berkeley, CA 94720. V. RADMILOVIC, Staff Scientist, and U. DAHMEN, Head, are with the National Center for Electron Microscopy, Lawrence Berkeley National Laboratory.

Manuscript submitted June 27, 2000.

Bulk alloys of Al-0.5 at. pct Si-0.5 at. pct Ge, Al-1 at. pct Si-l at. pct Ge-2 at. pct Cu, and Al-0.5 at. pct Si-0.5 at. pct Ge-2.5 at. pct Cu were made by arc melting, 99.999 (wt pct) Si, 99.9999 (wt pct) Ge, 99.999 (wt pct) Cu, and 99.99 (wt pct) Al. The cast samples were cold swaged to achieve 10 to 15 pct plastic deformation. They were then encapsulated in a sealed quartz glass tube that was back-filled with argon and annealed for 24 hours at 500 °C. From that temperature, they were quenched into an ice water bath. The final shape of the bulk alloy was roughly cylindrical, approximately 20 mm in length and 10 mm in diameter. The cylindrical ingots were sliced into discs 0.5 cm in thickness cut normal to the cylinder axis. The samples were aged at 190 °C. The temperature was monitored with an external thermocouple and varied no more than 1 °C. Hardness tests were done with a Rockwell hardness tester using the "B" scale (1/16th-in. steel ball, 100 kg load). Rockwell "B" values were converted to Brinell hardness using the appropriate ASTM standard.[21]

Analysis by vacuum emission spectroscopy on Al-0.5 at. pct Si-0.5 at. pct Ge-2.5 at. pct Cu and Al-0.5 at. pct Si-0.5 at. pct Ge (at FTI Anamet Laboratories, Hayward, CA) produced a composition of Al-0.48 at. pct Si-0.49 at. pct Ge-2.48 at. pct Cu and Al-0.55 at. pct Si-0.5 at. pct Ge with no other elements present in quantities greater than 0.005 pct.

The TEM samples were made from 200-μm-thick slices cut from the tested specimens. The cuts were made with a diamond saw using a low cutting speed and ample cooling fluid to minimize sample heating. The slices were ground down to a thickness between 125 and 150 μm using a 2400 grit silicon carbide polishing paper. They were then electrochemically polished in a Struers Tenupol-3 jet polisher at a temperature of -25 °C with a polishing voltage of 12.5 V. The polishing solution was 75 pct methanol $-$ 25 pct HNO_3 by volume.

Conventional TEM was performed using a JEOL* 200 CX at 200 kV. High-resolution TEM was performed on a PHILIPS** CM300-FEG operated at 300 kV.

*JEOL is a trademark of Japan Electron Optics Ltd., Tokyo.

**PHILIPS is a trademark of Philips Electronic Instrument Corp., Mahwah, NJ.

Figure 1 shows the hardening curves for the two alloys, Al-2Cu-1Si-1Ge and Al-2.5Cu-0.5Si-0.5Ge. The hardening curves show the rapid hardening, high peak strength, and thermal stability of the Al-Si-Ge-Cu alloys. Note that the alloy with the higher Cu content exhibits higher peak hardness than the alloy with the higher (Si,Ge) content.

Hardening curves for alloy 2219 (Al-2.8 at. pct Cu-0.15Mn-0.05Zr-0.055V-0.035Ti)[22] and for alloy 2014 (Al-1.94 at. pct Cu-0.8Si-0.4Mn-0.6Mg)[23] are included in the plot for comparison. Alloys 2219 and 2014 are used for comparison since they represent two Al-Cu based alloys known to exhibit high strength in their T-6 (solutionized, quenched, and artificially aged) condition.

At 190 °C, alloy 2014, which is not known to display high-temperature stability, quickly deteriorates. It should be noted that by aging 2014 at 160 °C for 13 hours, it is possible to obtain a Brinell Hardness of 122. However, even at 160 °C the alloy overages relatively quickly.

The alloy that is known for its high-temperature stability

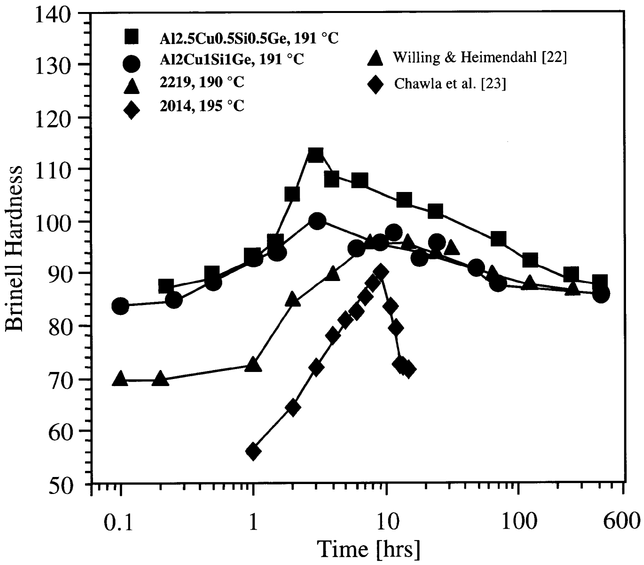

Fig. 1—Precipitation hardening in Al-Cu based alloys isothermally aged near 190 °C.

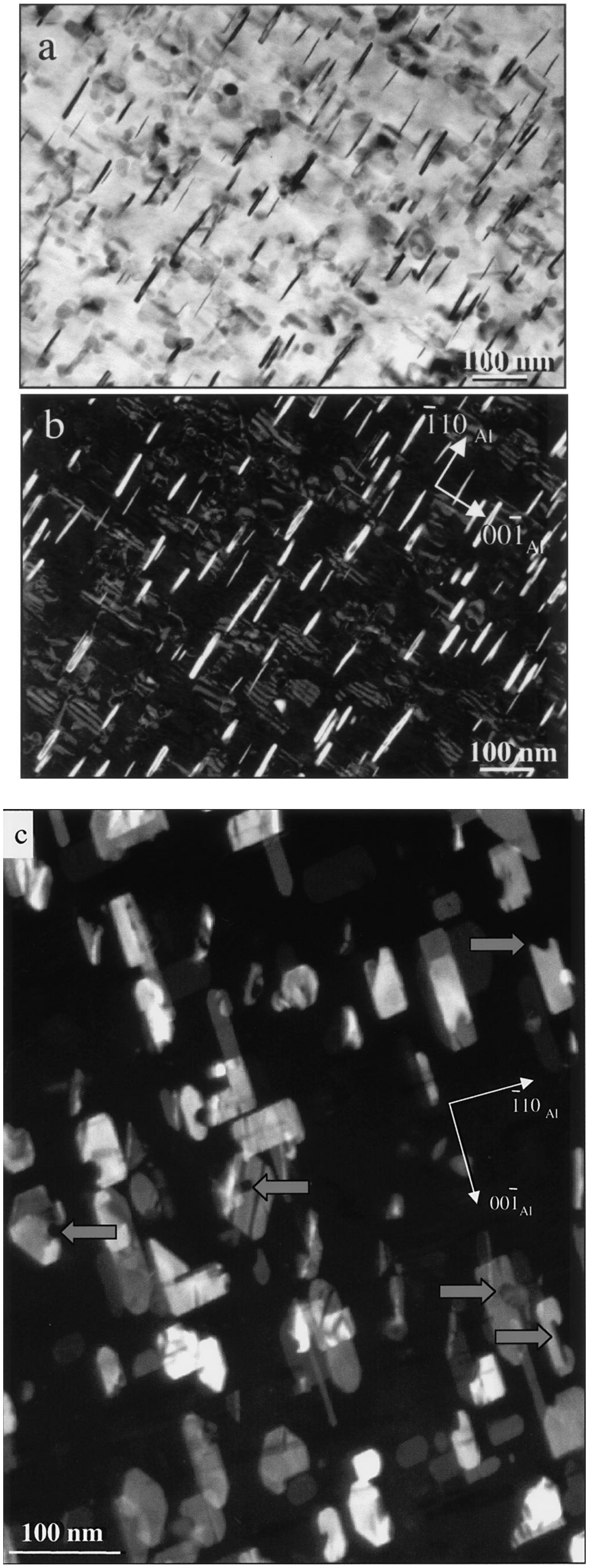

Fig. 2—Al-2Cu-1 at. pct Si-1 at. pct Ge alloy aged for 3 h at 190 °C. (*a*) Bright-field image near $[110]_{Al}$ zone axis. Dark-field images of θ' precipitates obtained using (*b*) $\bar{1}1\bar{2}_{\theta'}$ and (*c*) $1\bar{1}2_{\theta'}$. Si-Ge nucleation sites for θ' are indicated by arrows.

is 2219.[22] The microstructure of 2219 consists of various dispersoids used to control grain size and θ' precipitates. Compared to 2219, both Al-Cu-Si-Ge alloys possess higher peak hardness. Also, they reach maximum hardness after only 3 hours, instead of the 8 hours required for 2219 to obtain optimum hardness. On prolonged aging, Al-Cu-Si-Ge alloys overage at a rate similar to 2219, and after approximately 400 hours at elevated temperature, the hardness of all three alloys decreases asymptotically to approximately 86 HB.

Figure 2 shows the microstructure of Al-2Cu-1Si-1Ge, after aging for 3 hours at 190 °C. Figure 2(a) is a bright-field image of the microstructure near the $[110]_{Al}$ zone axis. Visible are both plates, identified in dark field (Figure 2(b)) as edge-on θ' and spherical Si-Ge particles. From Figures 2(a) and (b), it can be observed that both phases are densely distributed and are relatively fine and uniform in size. Figure 2(c) shows a dark-field image of the θ' precipitates oriented approximately 35 deg to the foil normal. They are imaged in the $[110]_{\theta'}$ zone axis, which is oriented 10 deg away from the $[110]_{Al}$ zone axis tilted along the 200 Kikuchi lines. The θ' precipitates are growing around the Si-Ge particles, giving the appearance in dark field of the θ' containing holes. The most dramatic examples of this are arrowed in the figure.

The juxtaposition of θ' and Si-Ge is illustrated in Figure 3, which is a high resolution image of two edge-on θ' precipitates (or a single one that was thinned from both sides) in contact with a multiply twinned Si-Ge particle. The sample was aged for 1 hour, and the image was taken in the $[001]_{Al}$ zone axis.

The twin segments B and D of Si-Ge particle in Figure 3 have the Baker–Nutting orientation relationship with aluminum matrix: $(100)_{Al}//(100)_{Si\text{-}Ge}$ and $[001]_{Al}//\ [011]_{Si\text{-}Ge}$. The heavy twinning of the Si-Ge precipitates may be due to the adsorption of different solute atoms at the diamond cubic/Al interface and their influence on the pattern of growth. Other adsorbed impurities, such as Na, Ba, Ca, or rare earth elements, have previously been observed to promote twinning in Al-Si.[24,25] But whatever the specific mechanism that causes the fine-scale multiple twinning, it seems clear that it is largely responsible for the equiaxed shapes of the Si-Ge particles.

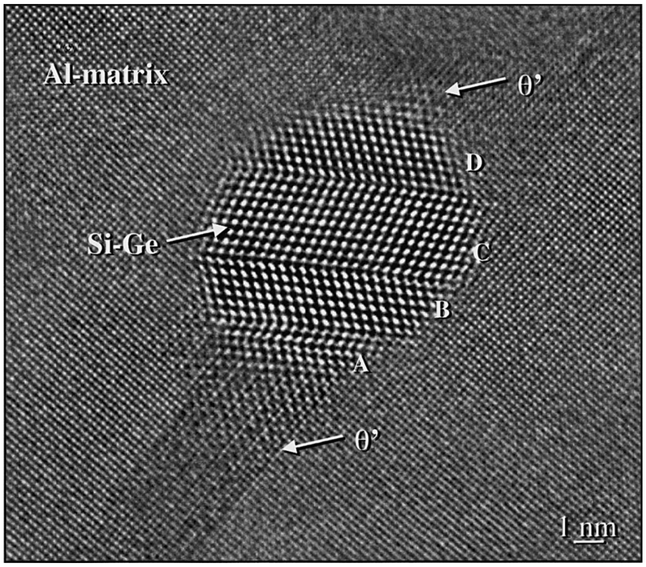

Fig. 3—High-resolution electron microscopy image of two θ' precipitates connected to a Si-Ge particle in Al-2Cu-1Si-1Ge alloy. Note that twin segments of Si-Ge, B, and D have a Baker–Nutting orientation relationship to the Al matrix: $(100)_{Al}//(110)_{Si\text{-}Ge}$ and $[001]_{Al}//[001]_{Si\text{-}Ge}$.

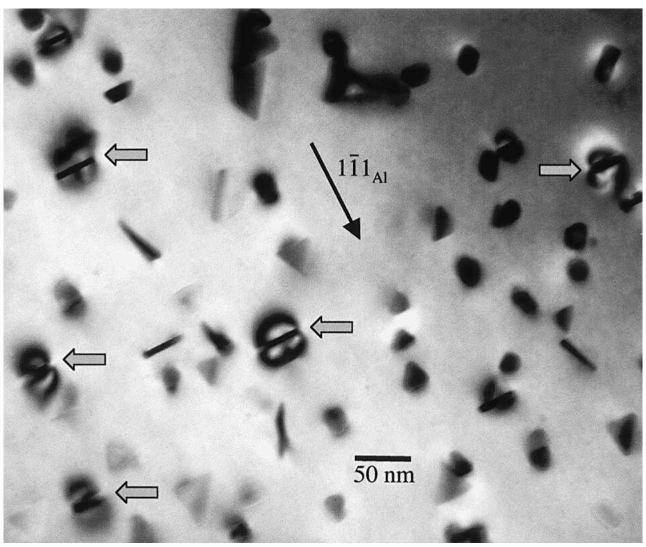

Fig. 4—Al-0.5 at. pct Si-0.5 at. pct Ge microstructure aged for 3 h. Image taken in $[110]_{Al}$ zone axis using a $1\bar{1}1_{Al}$ reflection.

In Figure 4, a two beam image of Al-0.5 at. pct Si-0.5 at. pct Ge aged 3 hours reveals that there is significant Ashby–Brown type strain[26] in the matrix around many of the Si-Ge particles. The particles showing the most pronounced matrix strain are arrowed. The strain is expected since the volume mismatch associated with the transformation of two Al unit cells into one Si or one Ge unit cell, $\Delta V/V_0$, is 20.6 and 36.4 pct, respectively ($a_{Si} = 5.43$ Å, $a_{Ge} = 5.66$ Å, and $a_{Al} = 4.05$ Å[27]). This results in a compressive transformation strain in the matrix of 6.85 pct and 12.1 pct. On the other hand, the nucleation of θ' results in a tensile coherency strain along its broad plate faces.[28] Thus, upon heterogeneous nucleation, strain compensation should result, lowering the overall energy.

Further work is needed to fully understand the precipitation sequence, age-hardening behavior, and thermal stability of this interesting alloy system.

The authors thank John Jacobsen, Chris Krenn, Andrew Minor, John Turner, and James Wu for technical assistance. This work was funded by the Director, Office of Energy Research, Office of Basic Energy Sciences, Materials Sciences Division, United States Department of Energy, under Contract No. DE-AC03-76SF00098. All TEM was performed at the National Center for Electron Microscopy.

REFERENCES

1. S.P. Ringer, K. Hono, I.J. Polmear, and T. Sakurai: *Acta Metall.*, 1996, vol. 44, pp. 1883-98.
2. R.N. Wilson: *J. Inst. Met.*, 1969, vol. 97, pp. 80-86.
3. V. Radmilovic, G. Thomas, G.J. Shiflet, and E.A. Starke: *Scripta Metall.*, 1989, vol. 23, pp. 1141-46.
4. J. Karov and W.V. Youdelis: *Mater. Sci. Technol.*, 1987, vol. 3, pp. 1-6.
5. S.K. Das, G. Thomas, and D. Rowcliffe: *Proc. 7th Int. Congr. on Electron Microscopy*, Grenoble, 1970, pp. 533-34.
6. S.P. Ringer, K. Hono, and T. Sakurai: *Metall. Mater. Trans. A*, 1995, vol. 26A, pp. 2207-18.
7. J.M. Silcock, T.J. Heal, and H.K. Hardy: *J. Inst. Met.*, 1955, vol. 84, pp. 23-31.
8. J.D. Boyd and R.B. Nicholson: *Acta Metall.*, 1971, vol. 19, pp. 1101-09.
9. R. Sankaren and C. Laird: *Mater. Sci. Eng.*, 1974, vol. 14, pp. 271-79.
10. A. Chitty: *J. Inst. Met.*, 1957–58, vol. 86, pp. 65-76.
11. D. Mitlin, V. Radmilovic, and J.W. Morris, Jr: *Metall. Mater. Trans. A*, 2000, vol. 31A, pp. 2697-2711.
12. I. Dutta, S.M. Allen, and J.L. Hafley: *Metall. Trans. A*, 1991, vol. 22A, 1991, pp. 2553-63.
13. T. Christman and S. Suresh: *Acta Metall.*, 1988, vol. 36, pp. 1691-04.
14. E. Hornbogen, A.K. Mukhopadhyay, and E.A. Strake, Jr.: *Z. Metallkd.*, 1992, vol. 83, pp. 577-84.
15. H.J. Koenigsmann, E.A. Starke, Jr., and P.E. Allire: *Acta Mater.*, 1996, vol. 44, pp. 3069-75.
16. H.J. Koeningsmann and E.A. Starke, Jr.: *Scripta Metall.*, 1996, vol. 35, pp. 1205-09.
17. E.A. Starke, Jr., G. Kralik, and V. Gerold: *Mater. Sci. Eng.*, 1973, vol. 11, pp. 319-23.
18. E. Hornbogen, A.K. Mukhopadhyay, and E.A. Starke, Jr.: *Scripta Metall. Mater.*, 1992, vol. 27, pp. 732-38.
19. E. Hornbogen, A.K. Mukhopadhyay, and E.A. Starke, Jr.: *J. Mater. Sci.*, 1993, vol. 28, pp. 3670-74.
20. D. Mitlin, M. Radmilovic, U. Dahmen, and J.W. Morris, Jr.: University of California, Berkeley, CA, unpublished research, May 2000.
21. *Annual Book of ASTM Standards*, ASTM, Philadelphia, PA, 1988, vol. 03.01, pp. 267-403.
22. V. Willig and M. von Heimendahl: *Z. Metallkd.*, 1979, vol. 70 (10), pp. 674-81.
23. K.K. Chawla, A.H. Esmaeili, A.K. Datye, and A.K. Vasudevan: *Scripta Metall.*, 1991, vol. 25, pp. 1315-19.
24. N. Cabrera and D.A. Vermilyea: *Growth and Perfection of Crystals*, Wiley, New York, NY, 1958, p. 394.
25. S.-Z. Lu and A. Hellawell: *Metall. Trans. A*, 1987, vol. 18A, pp. 1721-33.
26. P. Hirsch, A. Howie, R.B. Nicholson, D.W. Pashley, and M.J. Whelan: *Electron Microscopy of Thin Crystals*, R.E. Krieger Publishing Co., Malabar, FL, 1977, pp. 317-52.
27. B.D. Cullity: *Elements of X-Ray Diffraction*, 2nd ed., Addison-Wesley Publishing Company, Inc., New York, NY, 1978, pp. 506-07.
28. A. Kelly and R.B. Nicholson: *Progr. Mater. Sci.*, 1963, vol. 10, pp. 151-391.